Electronic Supplementary Information (ESI)

Through-Space Charge Transfer Dendrimers Employing Oxygen-Bridged Triarylboron Acceptors for Efficient Deep-Blue Electroluminescence

Baoyun Du,[a,b] Xingdong Wang,[a] Fan Chen,[a,b] Qingqing Yang,[a] Shiyang Shao,*[a] Lixiang Wang,*[a] Xiabin Jing[a] and Fosong Wang[a]

[a] State Key Laboratory of Polymer Physics and Chemistry, Changchun Institute of Applied Chemistry, Chinese Academy of Sciences, Changchun 130022, P. R. China

[b] School of Applied Chemistry and Engineering, University of Science and Technology of China, Hefei, Anhui 230026, P. R. China.

Experimental Details

General information. The chemicals and reagents were obtained from commercial sources (TCI (Shanghai), SigmaAldrich (China) and Energy Chemical (Beijing)) and were used directly. *N*, *N*-dimethylformamide (DMF) and 1,3-dimethyl-2-imidazolidinone (DMI) were dried by CaH_2, while tetrahydrofuran (THF) and 1,4-dioxane were distilled from sodium/benzophenone before use. Synthesis of **1**[1] and **5**[2] has been reported in literatures. ^{1}H、^{13}C and ^{19}F NMR spectra were recorded by Bruker Avance NMR spectrometers in $CDCl_3$ with tetramethylsilane (TMS) as the internal standard. Matrix-assisted laser desorption/ ionization time of flight (MALDI-TOF) mass spectra was measured on AXIMA CFR MS apparatus (COMPACT). Thermal gravimetric analysis (TGA) was performed on Perkin-Elmer-TGA 7. Cyclic voltammetry (CV) was carried out in electrochemical workstation (CHI610E) with a typical three-electrode cell using *n*-Bu_4NClO_4 (0.1 M) as supporting electrolyte and ferrocene as external reference. The oxidation and reduction curves were recorded in dichloromethane and DMF respectively, with dendrimer concentration of 5.0 mg/mL and scan rate of 50 mV/s. The highest occupied molecular orbital (HOMO) and the lowest unoccupied molecular orbital (LUMO) energy levels of the compounds were calculated

according to equations of $E_{HOMO}/E_{LUMO} = -(4.80 + E_{onset,\ ox}/E_{onset,\ red})$, in which $E_{onset,\ ox}$ and $E_{onset,\ red}$ are the onset of oxidation and reduction potentials respectively.

Photophysical measurements. UV-visible absorption was measured by PerkinElmer Lambda 35 UV-vis spectrometer, and photoluminescence (PL) spectra was measured by PerkinElmer LS 50B spectrofluorometer, respectively. PL decay curves were detected on Edinburgh fluorescence spectrometer (FLSP-980). The absolute PLQY values were measured by integrating sphere on Hamamatsu Photonics C9920-2 with excitation wavelength of 350 nm.

Computational method. The calculations were performed with Gaussian 09 package[3] using density functional theory (DFT) for ground state configuration optimization (B3LYP/6-31G(d)), and time-dependent density functional theory (TD-DFT) for excited state energy, natural transition orbitals (NTO) and IFCT analysis (PBE38/6-31G(d)). PBE38 is chosen as the function for TD-DFT calculation because its Hartree−Fock (HF) fraction (38.5%) is close to the optimal HF% for TAcBO-H (38.8%) and TAcBO-F (39.7%) according to the optimal Hartree−Fock (OHF) method established for donor-acceptor systems.[17] The optimal HF% (OHF%) is determined by OHF% = 42*q*,[17] where *q is* the amount (q) of charge transfer from donor to acceptor calculated by Multiwfn package (version 3.7),[5] and is 0.923 and 0.946 for TAcBO-H and TAcBO-F respectively. The reduced density gradient (RDG) analysis[4] were performed by Multiwfn[5] and RDG isosurface map was drawn by VMD software (version 1.9.3).

Fabrication of solution-processed OLEDs. Solution-processed OLEDs were fabricated with device configuration of ITO/PEDOT:PSS (40 nm) /dendrimer doped (5 or 10 wt%) in Ac6 (40 nm) /TSPO1 (8 nm) /TmPyPB (42 nm) /LiF (1 nm) /Al (100 nm). The glass substrates coated with indium tin oxide (ITO) (15 Ω per square) were washed with acetone, isopropanol and deionized water in sequence, and were dried under 120 ^{o}C for 45 min. Afterwards the substrates were treated by ultraviolet-ozone for 45 min. PEDOT:PSS (Clevious P AI4083) was spin-coated on the substrates to form a film with thickness of 40 nm, and annealed at 120 ^{o}C for 1 h. After transferring the substrates into glovebox filled with N_2, solutions of dendrimers in chlorobenzene (10 mg/mL) were spin-coated (1500 rpm) on PEDOT:PSS layer at room temperature to form the emissive layer. Then TSPO1 and TmPyPB was evaporated successively on top of the emissive layer in a vacuum chamber at a pressure less than 4×10^{-4} Pa with deposition rate of 0.6 Å/s and 1.2

Å/s, respectively. LiF and Al were then deposited as the cathode with deposition rate of 0.2 Å/s and 3.3 Å/s, respectively, providing the device with individual pixel size of 0.14 cm^2 (0.35 cm*0.40 cm). The *J*–*V*–*L* characteristics of the OLEDs were measured using Keithley 2400/2000 source meter. EL spectra were measured by a PR650 spectra colorimeter. EQE of the devices were calculated based on the *J*–*L* characteristics.

Synthetic procedures

Scheme S1. Synthetic route for TAcBO-H and TAcBO-F.

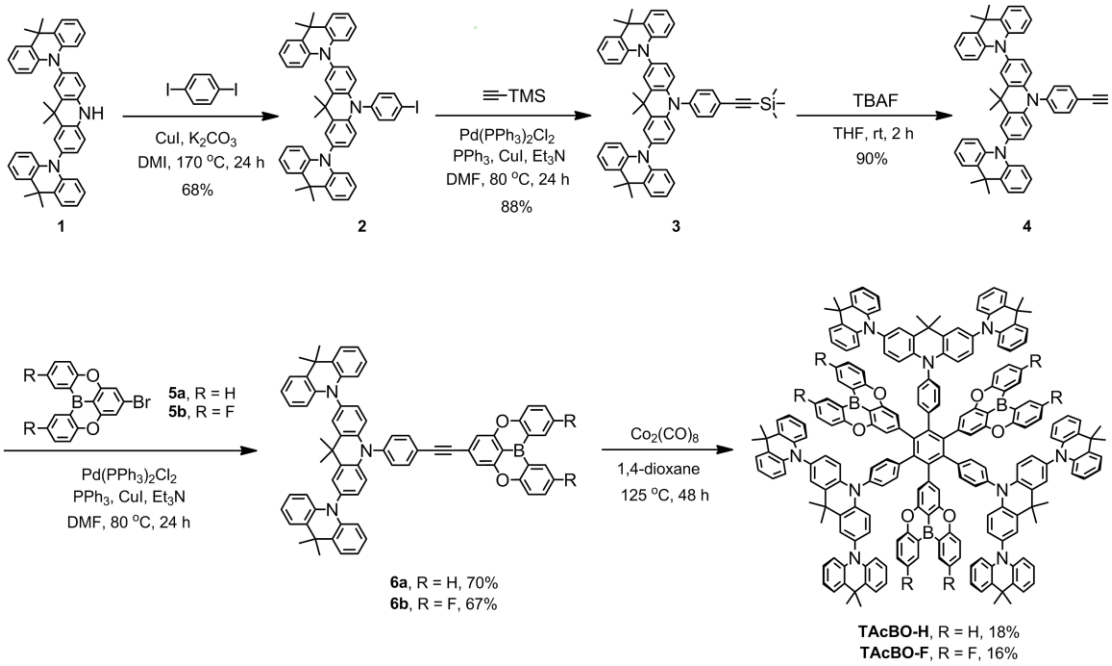

10′-(4-iodophenyl)-9,9,9′,9′,9″,9″-hexamethyl-teracridan (2)

A mixture of 9,9,9′,9′,9″,9″-hexamethyl-teracridan (**1**) (25.0 g, 40.0 mmol), 1, 4-diiodobenzene (14.5 g, 44.0 mmol), CuI (2.3 g, 12.0 mmol) and K_2CO_3 (8.3 g, 60.0 mmol) in 1,3-dimethyl-2-imidazolidinone (DMI) (500 mL) was stirred at 170 ℃ for 24 h. After cooling to room temperature, the mixture was poured into deionized water (2000 mL) and extracted by chloroform three times (400 mL ×3). After drying the combined organic phase with anhydrous $MgSO_4$, the solvent was removed under vacuum and the residue was purified by silica gel column chromatography (petroleum ether/ dichloromethane=5/1, v/v) to afford the product as a white solid (22.5 g, 68%). ^{1}H NMR (400 MHz, $CDCl_3$) δ 8.07 (d, *J* = 8.5 Hz, 2H), 7.47 (dd, *J* = 7.7, 1.5 Hz, 4H), 7.42 (d, *J* = 2.2 Hz, 2H), 7.32 (dd, *J* = 8.9, 2.1 Hz, 2H), 7.00 (m, 6H), 6.94 (t, *J* = 6.0 Hz, 4H), 6.56 (d, *J* = 8.6 Hz, 2H), 6.36 (dd, *J* = 8.1, 1.0 Hz, 4H), 1.72 (s, 12H), 1.68 (s, 6H). ^{13}C NMR (126 MHz, $CDCl_3$) δ 141.21, 140.52, 140.07, 134.22, 133.30, 132.41, 129.88, 129.10, 127.79, 126.36, 125.27, 120.34, 116.03, 113.97.

9,9,9′,9′,9″,9″-hexamethyl-10′-(4-((trimethylsilyl)ethynyl)phenyl)-teracridan (3)

Under argon atmosphere, **2** (21.5 g, 26.0 mmol), trimethylsilylacetylene (3.1 g, 31.2 mmol), bis(triphenylphosphine)palladium(II) chloride ($Pd(PPh_3)_2Cl_2$, 365.0 mg, 0.52 mmol), CuI (99.3

mg, 0.52 mmol), triphenylphosphine (PPh_3, 272.8 mg, 1.04 mmol), triethylamine (Et_3N, 50 mL) and DMF (100 mL) were added into a Schlenk flask. The mixture was heated at 80 ℃ for 24 h, then poured into dilute hydrochloric acid (1 mol/L, 500 mL). After filtration, the filter residue was washed with deionized water and dried under vacuum. The filter residue was purified by silica gel column chromatography (petroleum ether/dichloromethane = 5:1, v/v) to afford the product as a white solid (18.2 g, 88%). ^{1}H NMR (400 MHz, $CDCl_3$) δ 7.80 (d, *J* = 7.6 Hz, 2H), 7.48 (d, *J* = 8.4 Hz, 2H), 7.43 (dd, *J* = 7.6, 1.6 Hz, 4H), 7.38 (d, *J* = 2.0 Hz, 2H), 7.0-6.89 (m, 10H), 6.51 (d, *J* = 8.8 Hz, 2H), 6.33 (dd, *J* =8.0, 1.2 Hz, 4H), 1.69 (s, 12H), 1.65 (s, 6H), 0.29 (s, 9H). ^{13}C NMR (126 MHz, $CDCl_3$) δ 141.32, 140.83, 140.25, 134.85, 134.24, 132.45, 131.30, 129.97, 129.14, 127.86, 126.45, 125.36, 123.89, 120.41, 116.15, 114.08, 104.03, 96.27,36.67, 36.03, 31.56, 30.90, 0.01.

10'-(4-ethynylphenyl)-9,9,9',9',9'',9''-hexamethyl-teracridan (4)

After dissolving **3** (16.0 g, 20.0 mmol) in THF (150 mL), tetrabutylammonium fluoride (TBAF, 1 mol/L in THF, 24 mL, 24.0 mmol) was added dropwise. After stirring for 2 h at room temperature, the mixture was added into dilute hydrochloric acid (1 mol/L, 200 mL). The mixture was filtered and the filter residue was washed with deionized water. After drying under vacuum, the filter residue was purified by silica gel column chromatography (petroleum ether/dichloromethane = 5:1, v/v) to afford the product as a white solid (13.0 g, 90%).^{1}H NMR (500 MHz, $CDCl_3$) δ 7.85 (d, *J* = 8.5 Hz, 2H), 7.53 (d, *J* = 8.5 Hz, 2H), 7.45 (dd, *J* = 7.5, 2.0 Hz, 4H), 7.41 (d, *J* = 2.0 Hz, 2H), 7.0-6.96 (m, 6H), 6.91 (t, *J* = 7.5 Hz, 4H), 6.55 (d, *J* = 8.5 Hz, 2H), 6.36 (d, *J* = 8.5 Hz, 4H), 1.71 (s, 12H), 1.68 (s, 6H). ^{13}C NMR (126 MHz, $CDCl_3$) δ 141.25, 141.15, 140.13, 134.96, 134.23, 132.43, 131.36, 129.91, 129.11, 127.81, 126.37, 125.27, 122.82, 120.35, 116.07, 114.00, 82.70, 78.78, 36.60, 35.95, 31.45, 30.84.

10'-(4-(5,9-dioxa-13b-boranaphtho[3,2,1-de]anthracen-7-ylethynyl)phenyl)-9,9,9',9',9'',9''-hexa methyl-teracridan (6a)

Under argon atmosphere, **4** (3.6 g, 5.0 mmol), 7-bromo-5,9-dioxa-13*b*-boranaphtho[3,2,1-*de*]anthracene (**5a**, 1.8 g, 5.0 mmol), $Pd(PPh_3)_2Cl_2$ (70.2 mg, 0.1 mmol), CuI (19.1 mg, 0.1 mmol), PPh_3 (52.6 mg, 0.2 mmol), Et_3N (25 mL) and DMF (50 mL) were added into a dry Schlenk flask. The mixture was heated at 80 ℃ for 24 h, then

the mixture was poured into dilute hydrochloric acid (1 mol/L, 50 mL). After filtration, the filter residue was washed with deionized water and dried under vacuum. The filter residue was purified by silica gel column chromatography (petroleum ether/dichloromethane = 4:1, v/v) to afford the product as a white solid (3.5 g, 70%).^{1}H NMR (500 MHz, $CDCl_3$) δ 8.69 (d, *J* = 7.5 Hz, 2H), 7.95 (d, *J* = 8.0 Hz, 2H), 7.72 (t, *J* = 7.0 Hz, 2H), 7.60-7.56 (m, 4H), 7.46-7.41 (m, 10H), 7.01-6.98 (t, *J* = 9.0 Hz, 6H), 6.90 (t, *J* = 7.5 Hz, 4H), 6.59 (d, *J* =8.5 Hz, 2H), 6.36 (d, *J* = 8.0 Hz, 4H), 1.70 (s, 12H), 1.67 (s, 6H). ^{13}C NMR (126 MHz, $CDCl_3$) δ 159.80, 156.54, 140.97, 140.60, 139.74, 134.32, 134.07, 133.59, 133.44, 131.98, 131.09, 129.60, 128.68, 128.20, 127.40, 126.03, 124.80, 122.90, 122.66, 121.70, 120.10, 118.09, 115.79, 114.55, 113.74, 111.23, 90.64, 90.41, 36.18, 35.54, 30.85, 30.55. MALDI TOF-MS: calcd for $C_{71}H_{54}BN_3O_2$: 991.4, found: 991.4 $[M]^+$.

10'-(4-((2,12-difluoro-5,9-dioxa-13b-boranaphtho[3,2,1-de]anthracen-7-yl)ethynyl)phenyl)-9,9,9',9',9'',9''-hexamethyl-9',10'-dihydro-teracridan (6b)

Under argon atmosphere, **4** (2.3 g, 3.2 mmol), 7-bromo-2,12-difluoro-5,9-dioxa-13*b*-boranaphtho[3,2,1-*de*]anthracene (**5b**, 1.2 g, 3.2 mmol), $Pd(PPh_3)_2Cl_2$ (45.0 mg, 0.064 mmol), CuI (12.2 mg, 0.064 mmol), PPh_3 (33.6 mg, 0.128 mmol), Et_3N (20 mL) and DMF (40 mL) were added into a dry Schlenk flask. The mixture was heated at 80 ℃ for 24 h, then the mixture was poured into dilute hydrochloric acid (1 mol/L, 50 mL). After filtration, the filter residue was washed with deionized water and dried under vacuum. The filter residue was purified by silica gel column chromatography (petroleum ether/dichloromethane = 4:1, v/v) afforded the product as a white solid (2.2 g, 67%). ^{1}H NMR (400 MHz, $CDCl_3$) δ 8.19 (dd, *J* = 8.8, 2.8 Hz, 2H), 7.96 (d, *J* = 8.4 Hz, 2H), 7.62-7.55 (m, 4H), 7.49-7.45 (m, 6H), 7.43 (s, 2H), 7.41 (d, *J* = 2.4 Hz, 2H), 7.02-6.97 (m, 6H), 6.90 (t, *J* = 7.2 Hz, 4H), 6.59 (d, *J* =8.8 Hz, 2H), 6.36 (dd, *J* = 9.2, 1.2 Hz, 4H), 1.70 (s, 12H), 1.68 (s, 6H). ^{13}C NMR (126 MHz, $CDCl_3$) δ 159.11, 157.17, 157.11, 156.49, 141.25, 140.17, 134.67, 134.26, 132.47, 131.55, 129.91, 129.35, 129.14, 127.84, 126.38, 125.29, 123.33, 121.91, 121.72, 120.36, 120.25, 118.29, 118.13, 116.10, 114.00, 111.59, 91.25, 90.39, 36.63, 35.95, 31.47, 30.83. ^{19}F NMR (471 MHz, $CDCl_3$) δ -119.42 (s, 2F). MALDI TOF-MS: calcd for $C_{71}H_{52}BF_2N_3O_2$: 1027.4, found: 1027.4 $[M]^+$.

TAcBO-H

A mixture of **6a** (2.0 g, 2.0 mmol), $Co_2(CO)_8$ (136.8 mg, 0.4 mmol) and 1,4-dioxane (20 mL) was

stirred at 125 ℃ for 48 h under argon atmosphere. After cooling to room temperature, the mixture was poured into water (100 mL) and the precipitation was filtered. This precipitation contains two main products with close R_f values of 0.30 and 0.33 respectively by thin layer chromatography (TLC) analysis (silica gel, petroleum ether/dichloromethane = 2:1, v/v). The precipitation was subjected to silica gel column chromatography (petroleum ether/dichloromethane = 3:1, v/v), and the product with R_f of 0.33 can be separated as pure compound, which was proved to be the desired compound TAcBO-H (white powder, 360.0 mg, 18%). Note that the other product with R_f of 0.30 (which may be the asymmetrical isomer according to previous report[18]) cannot be separated as pure compound by us because it was mixed with TAcBO-H and some other unknown impurities although different purification methods (column chromatography, extraction and precipitation) were tried. Characterization data for TAcBO-H: ^{1}H NMR (500 MHz, $CDCl_3$) δ 8.00 (d, *J*=8.0 Hz, 6H), 7.48 (d, *J*=8.0 Hz, 6H), 7.43 (d, *J*=7.5 Hz, 12H), 7.23 (d, *J*=8.5 Hz, 6H), 7.08 (d, *J*=7.5 Hz, 12H), 7.06 (s, 6H), 6.87 (t, *J*=7.5 Hz, 12H), 6.84 (t, *J*=7.5 Hz, 6H), 6.78 (t, *J*=7.0 Hz, 12H), 6.66 (t, *J* =7.0 Hz, 6H), 5.96 (d, *J*=8.5 Hz, 12H), 5.83 (d, *J*=8.5 Hz, 6H), 5.50 (d, *J* =9.0 Hz, 6H), 1.68 (s, 36H), 1.40 (s, 18H). ^{13}C NMR (126 MHz, $CDCl_3$) δ 160.16, 156.52, 146.84, 141.26, 140.54, 140.42, 140.30, 139.78, 134.35, 133.66, 133.61, 133.43, 131.53, 130.38, 129.59, 128.83, 127.08, 126.18, 124.79, 122.88, 121.71, 120.04, 118.87, 117.85, 115.30, 114.04, 112.75, 112.25, 36.28, 35.86, 31.21, 30.72. MALDI TOF-MS: calcd for $C_{213}H_{162}B_3N_9O_6$: 2976.1, found: 2976.1 $[M]^+$.

TACBO-F

A mixture of **6b** (1.9 g, 1.8 mmol), $Co_2(CO)_8$ (123.1 mg, 0.36 mmol) and 1,4-dioxane (20 mL) was stirred at 125 ℃ for 48 h under argon atmosphere. After cooling to room temperature, the mixture was poured into water (100 mL) and the precipitation was filtered. This precipitation also contains two main products with close R_f values of 0.28 and 0.30 respectively by TLC analysis (silica gel, petroleum ether/dichloromethane = 2:1, v/v), and only the product with R_f of 0.30 can be separated as pure compound by silica gel column chromatography (petroleum ether/dichloromethane = 3:1, v/v), affording TAcBO-F as light-green powder (288.0 mg, 16%). ^{1}H NMR (400 MHz, $CDCl_3$) δ 7.51(dd, *J*=6.8, 2.4 Hz, 6H), 7.48-7.45 (m, 18H), 7.20 (dd, *J*=7.2, 3.6 Hz, 12H), 7.13-7.10 (m, 6H), 7.07 (s, 6H), 6.92 (t, *J*=6.4 Hz, 12H), 6.78 (t, *J*=6.4 Hz, 12H), 6.56 (t,

J =6.5 Hz, 6H), 5.96(d, *J*=6.4 Hz, 12H), 5.83 (d, *J*=8.0 Hz, 6H), 5.60 (dd, *J* =7.2, 1.6 Hz, 6H), 1.67 s, 36H), 1.43(s, 18H). ^{13}C NMR (126 MHz, $CDCl_3$) δ 158.85, 156.55, 156.42, 156.24, 147.33, 141.25, 140.47, 140.32, 139.70, 138.85, 133.56, 131.66, 130.89, 130.51, 129.99, 128.79, 127.29, 125.98, 124.93, 121.84, 121.60, 120.24, 119.57, 118.24, 115.19. 113.73, .112.31, 111.82, 36.32, 35.93, 30.71, 29.69. ^{19}F NMR (471 MHz, $CDCl_3$) δ -117.66 (s, 6F). MALDI TOF-MS: calcd for $C_{213}H_{156}B_3F_6N_9O_6$: 3084.0, found: 3084.0 $[M]^+$.

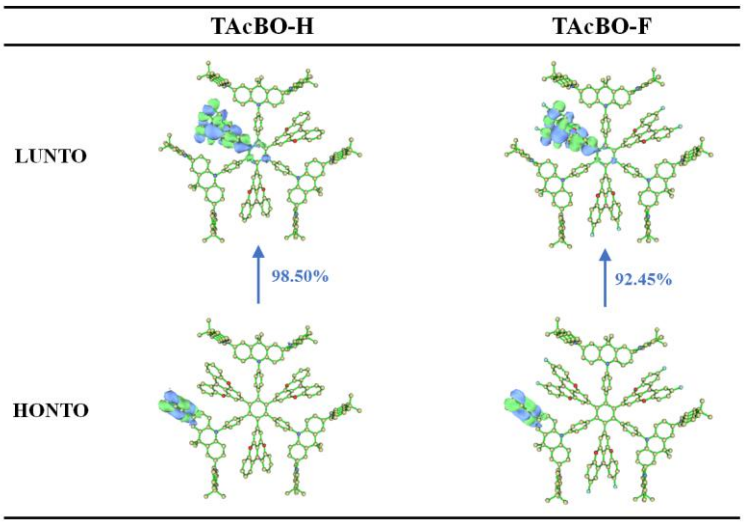

Figure S1. Natural transition orbitals (NTOs) for S_0-S_1 transition of TAcBO-H and TAcBO-F by TD-DFT calculation. (HONTO and LUNTO refer to highest occupied and lowest unoccupied NTOs respectively.)

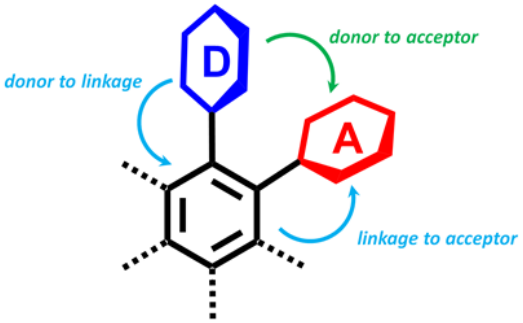

Emitter	TAcBO-H	TAcBO-F
η (donor to acceptor)	0.88206	0.92205
η (donor to linker)	0.07713	0.05191
η (linker to acceptor)	0.00003	0.00001

Figure S2. Contribution ratio (η) for electron transfer from donor to acceptor, donor to linker (central phenyl ring), and linker to acceptor for $S_0 \rightarrow S_1$ transition by interfragment charge transfer (IFCT) analysis using Multiwfn (version 3.7) package.

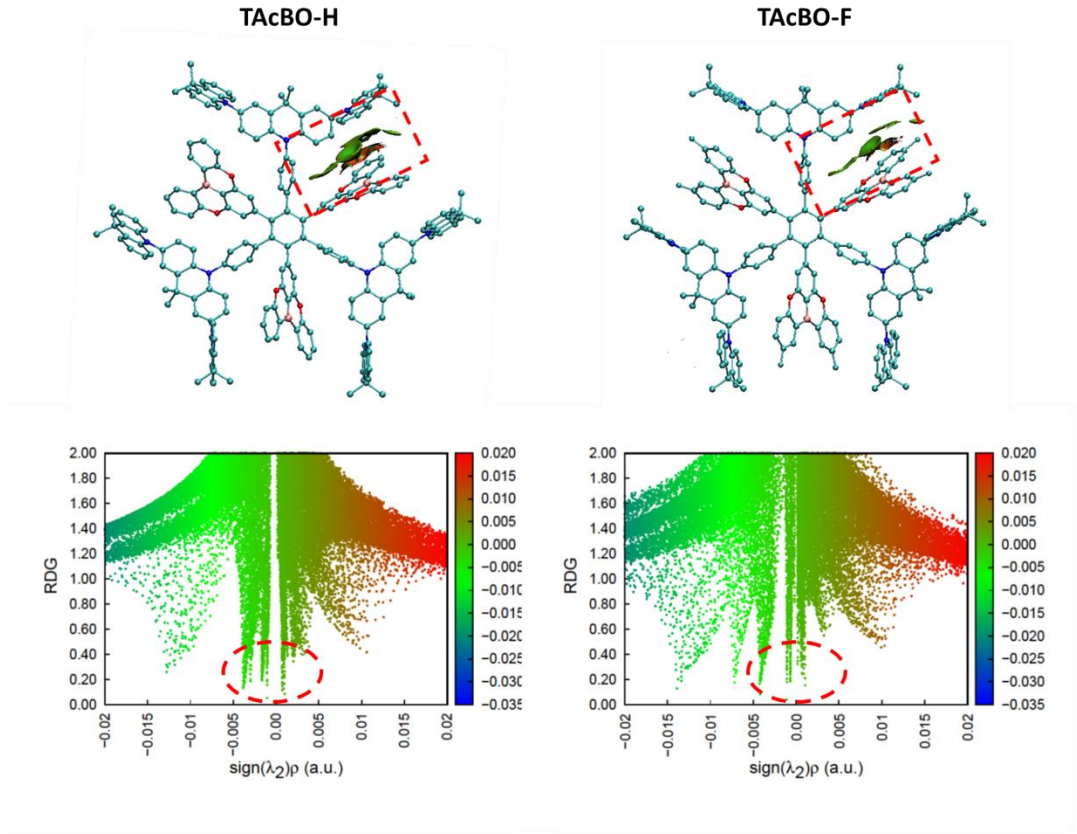

Figure S3. Reduced density gradient (RDG) isosurface map (isovalue=1.30) and corresponding scatter diagram (plots of RDG to sign(λ_2) ρ) for TAcBO-H and TAcBO-F. The green region (in red dashed box) and the spikes region (in red dashed circles) show the noncovalent through-space π-π interactions between donor and acceptor.

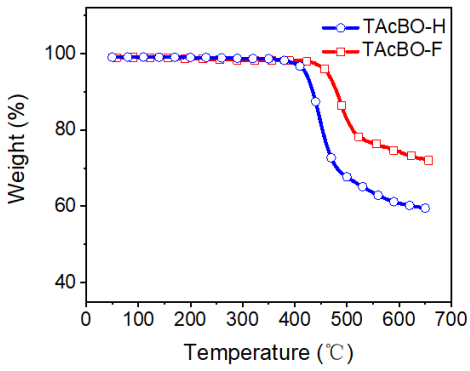

Figure S4. Thermogravimetric analysis (TGA) curves for TAcBO-H and TAcBO-F.

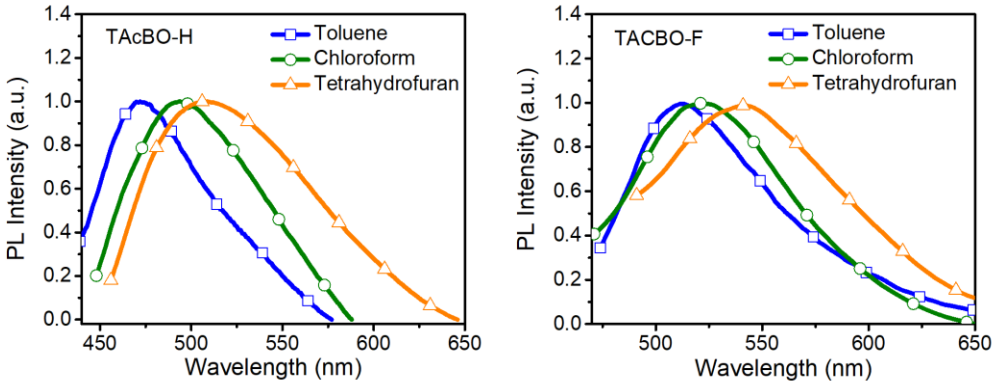

Figure S5. PL spectra of TAcBO-H and TAcBO-F in solvents with different polarity (10^{-4} mol L^{-1}).

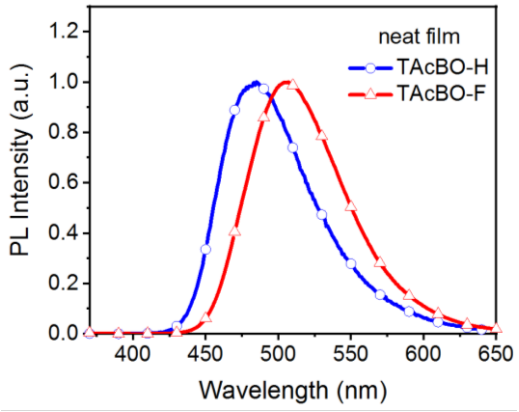

Figure S6. PL spectra for neat films of TAcBO-H and TAcBO-F.

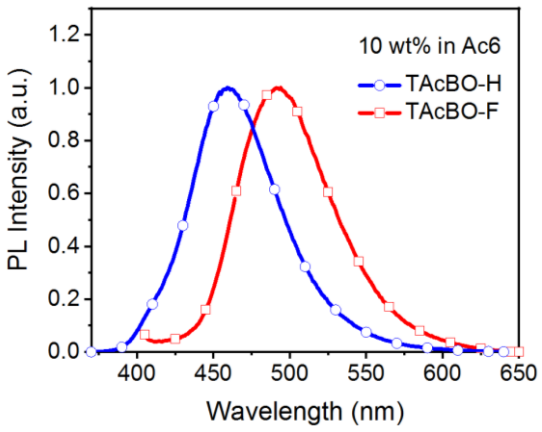

Figure S7. PL spectra for doped films of TAcBO-H and TAcBO-F in Ac6 (doping concentration: 10 wt%).

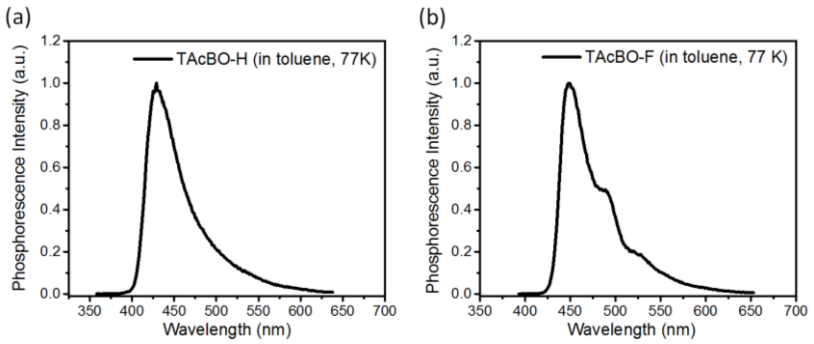

Figure S8. Phosphorescent spectra of TAcBO-H and TAcBO-F in toluene at 77K (delay time: 2 ms, integration time: 2 ms).

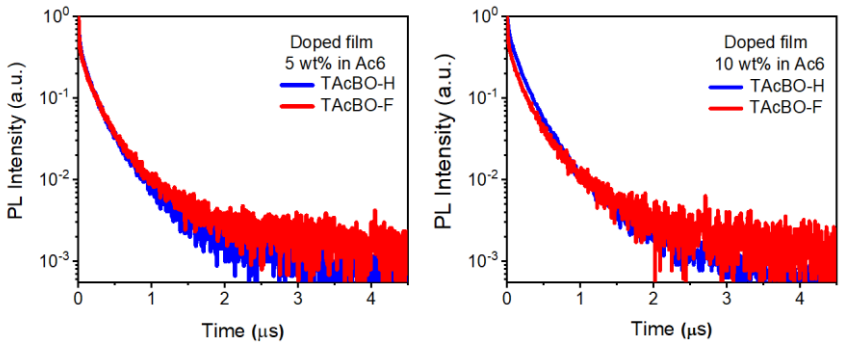

Figure S9. Transient PL decay profiles of TAcBO-H and TAcBO-F in doped film.

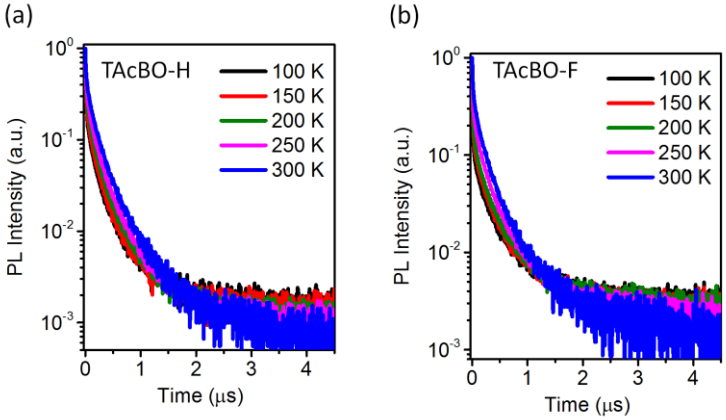

Figure S10. Temperature-dependent PL decay characteristics for TAcBO-H and TAcBO-F in doped films (5 wt% in Ac6).

Table S1. Summary of physical properties for TAcBO-H and TAcBO-F.

Dendrimer	λ_{em} [a] (nm)	τ_p/τ_d [b] (μs/μs, tol)	τ_p/τ_d [b] (μs/μs, film)	PLQY[c] (%)	k_{RISC} [d] ($\times10^6$ s^{-1})	$E_{onset,\ ox}/E_{onset,\ red}$ [e] (V)	HOMO/LUMO[f] (eV)	S_1/T_1 [g] (eV)	ΔE_{ST} [h] (eV)
TAcBO-H	453	0.010/0.30	0.012/0.18	70 (56)	2.7	0.30/-2.04	-5.10/-2.76	2.98/2.89	0.09
TAcBO-F	489	0.013/0.31	0.010/0.19	85 (68)	5.2	0.30/-1.91	-5.10/-2.89	2.84/2.76	0.08

[a] Emission peak in doped film (5 wt% in Ac6). [b] Lifetimes of prompt fluorescence (τ_p) and delayed fluorescence (τ_d) in toluene and doped film at 300 K under vacuum. [c] PL quantum yield for doped film (5 wt% in Ac6) and neat film (in parentheses). [d] RISC rate constants calculated according to the following equations[6]: $k_p=1/\tau_p$, $k_d=1/\tau_d$, $k_{ISC}=(1-\Phi_p)k_p$, $k_{RISC}=(k_Pk_d/k_{ISC})(\Phi_{DF}/\Phi_{PF})$, where k_p and k_d are decay rate constants of prompt and delayed fluorescence respectively, k_{ISC} is intersystem crossing rate constant from S_1 to T_1 state, and Φ_{DF} and Φ_{PF} are PLQY for delayed and prompt fluorescence respectively. [e] Onset of oxidation and reduction potential respectively. [f] HOMO and LUMO levels determined by $E_{onset,\ ox}$ and $E_{onset,\ red}$ respectively. [g] Lowest singlet/triplet energy from fluorescence/phosphorescence spectra in toluene. [h] Singlet-triplet energy gap.

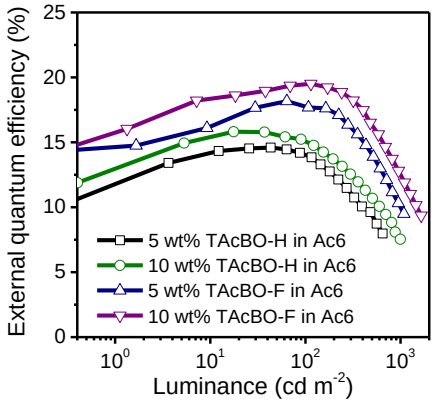

Figure S11. EQE–*L* characteristics for solution-processed OLEDs based on TSCT dendrimers.

Table S2. Device performance for solution-processed OLEDs based on TAcBO-H and TAcBO-F.

Dendrimer	**V_{on} [a] (V)**	**LE [b] ($cd\ A^{-1}$)**	**EQE [c] (%)**	**L_{max} [d] ($cd\ m^{-2}$)**	**CIE [e] (x, y)**
		Maximum value/at 100 cd m^{-2}/at 500 cd m^{-2}			
5 wt% TAcBO-H	3.1	19.4/18.4/12.8	14.6/13.8/9.6	1637	0.16, 0.14
10 wt% TAcBO-H	3.1	23.1/22.0/15.6	15.8/15.0/10.7	1850	0.16, 0.16
5 wt% TAcBO-F	3.0	46.7/45.5/35.7	18.2/17.6/13.9	3160	0.20, 0.41
10 wt% TAcBO-F	3.0	52.0/51.8/44.0	19.5/19.4/16.5	3439	0.20, 0.43

[a] Turn-on voltage at luminance of 1 cd m^{-2}. [b] Luminous efficiency. [c] External quantum efficiency. [d] Maximum luminance. [e] CIE coordinates at 4 V.

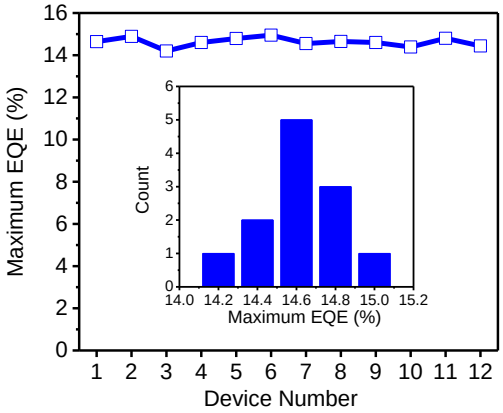

Figure S12. Maximum EQEs for solution-processed OLEDs using TAcBO-H (5 wt% in Ac6) as emitter measured from 12 devices. The average maximum EQE is 14.63% with distribution from 14.20% to 14.95%, corresponding to variation of ±0.43%.

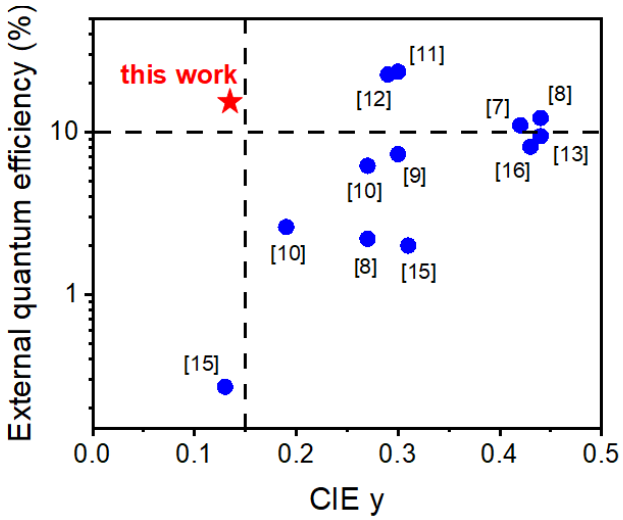

Figure S13. EL performance for TAcBO-H in this work and blue TADF dendrimers in literatures.

Table S3. List of EL performance for blue TADF dendrimers reported in this work and literatures.

Emitter	V_{on} (V)	LE_{max} (cd A^{-1})	EQE_{max} (%)	CIE (x, y)	Reference
TAcBO-H	3.1	19.4	14.6	0.16, 0.14	this work
Ac3TRZ3	2.9	30.3	11.0	0.22, 0.42	[7]
CzDMAC-DPS	3.6	30.6	12.2	0.22, 0.44	[8]
DCzDMAC-DPS	5.2	3.8	2.2	0.18, 0.27	[8]
POCz-DPS	5.4	12.6	7.3	0.18, 0.30	[9]
tbCz-SO	5.1	4.0	2.6	0.16, 0.19	[10]

poCz-SO	6.1	10.5	6.2	0.18, 0.27	[10]
Cz-4CzCN: Cz-4CzCN	3.5	48.6	23.5	0.15, 0.30	[11]
PCz-4CzCN	2.8	45.2	22.6	0.16, 0.29	[12]
5CzBN-Cz	3.5	27.03	9.42	0.21, 0.44	[13]
G2	4.8	4.1	--	0.15, 0.12	[14]
G3	5.2	1.07	--	0.19, 0.15	[14]
TPPOCz	4.3	0.2	0.27	0.18, 0.13	[15]
TPPOCz/TmPyPB	6.2	3.2	2.0	0.26, 0.31	[15]
TB14CZ-ACTRZ	4.5	20.7	8.1	0.22, 0.43	[16]

References

[1] Q. Li, J. Hu, J. Lv, X. Wang, S. Shao, L. Wang, X. Jing and F. Wang, *Angew. Chem. Int. Ed*, **2020**, 59, 20174-20182.

[2] F. Chen, J. Hu, X. Wang, S. Shao, L. Wang, X. Jing and F. Wang, *Sci China Chem*, **2020**, 63, 1112-1120.

[3] Frisch, M. J. et al. Gaussian 09, Revision C.01. (Gaussian, 2010).

[4] E. R. Johnson, S. Keinan, P. Mori-Sánchez, J. Contreras-García, A. J. Cohen, W. Yang, *J. Am. Chem. Soc.* **2010**, *132*, 6498.

[5] T. Lu and F. Chen, *J Comput Chem*, **2012**, 33, 580-592.

[6] N. Ikeda, S. Oda, R. Matsumoto, M. Yoshioka, D. Fukushima, K. Yoshiura, N. Yasuda and T. Hatakeyama, *Adv. Mater*, **2020**, 32, 2004072.

[7] X. Wang, S. Wang, J. Lv, S. Shao, L. Wang, X. Jing and F. Wang, *Chem Sci*, **2019**, 10, 2915-2923.

[8] J. Luo, S. Gong, Y. Gu, T. Chen, Y. Li, C. Zhong, G. Xie and C. Yang, *J. Mater. Chem. C*, **2016**, 4, 2442-2446.

[9] X. Ban, W. Jiang, K. Sun, B. Lin and Y. Sun, *ACS Appl Mater Interfaces*, **2017**, 9, 7339-7346.

[10] X. Ban, B. Lin, W. Jiang and Y. Sun, *Chem Asian J*, **2017**, 12, 216-223.

[11] X. Ban, A. Zhu, T. Zhang, Z. Tong, W. Jiang and Y. Sun, *Chem. Commun*, **2017**, 53, 11834-11837.

[12] X. Ban, Y. Liu, J. Pan, F. Chen, A. Zhu, W. Jiang, Y. Sun and Y. Dong, *ACS Appl Mater Interfaces*, **2020**, 12, 1190-1200.

[13] D. Liu, W. Tian, Y. Feng, X. Zhang, X. Ban, W. Jiang and Y. Sun, *ACS Appl Mater Interfaces*, **2019**, 11, 16737-16748.

[14] J. Li, X. Liao, H. Xu, L. Li, J. Zhang, H. Wang and B. Xu, *Dyes and Pigments*, **2017**, 140, 79-86.

[15] J. Wang, J. Peng, W. Yao, C. Jiang, C. Liu, C. Zhang, M. He, R. Liu, X. Xia and C. Yao, *Org. Electron*, **2017**, 48, 262-270.

[16] M. Godumala, S. Choi, H. J. Kim, C. Lee, S. Park, J. S. Moon, K. Si Woo, J. H. Kwon, M. J. Cho and D. H. Choi, *J. Mater. Chem. C*, **2018**, 6, 1160-1170.

[17] S. Huang, Q. Zhang, Y. Shiota, T. Nakagawa, K. Kuwabara, K. Yoshizawa, C. Adachi, *J. Chem. Theory Comput.* **2013**, *9*, 3872.

[18] M. Steeger, C. Lambert, *Chem. Eur. J.* **2012**, *18*, 11937.

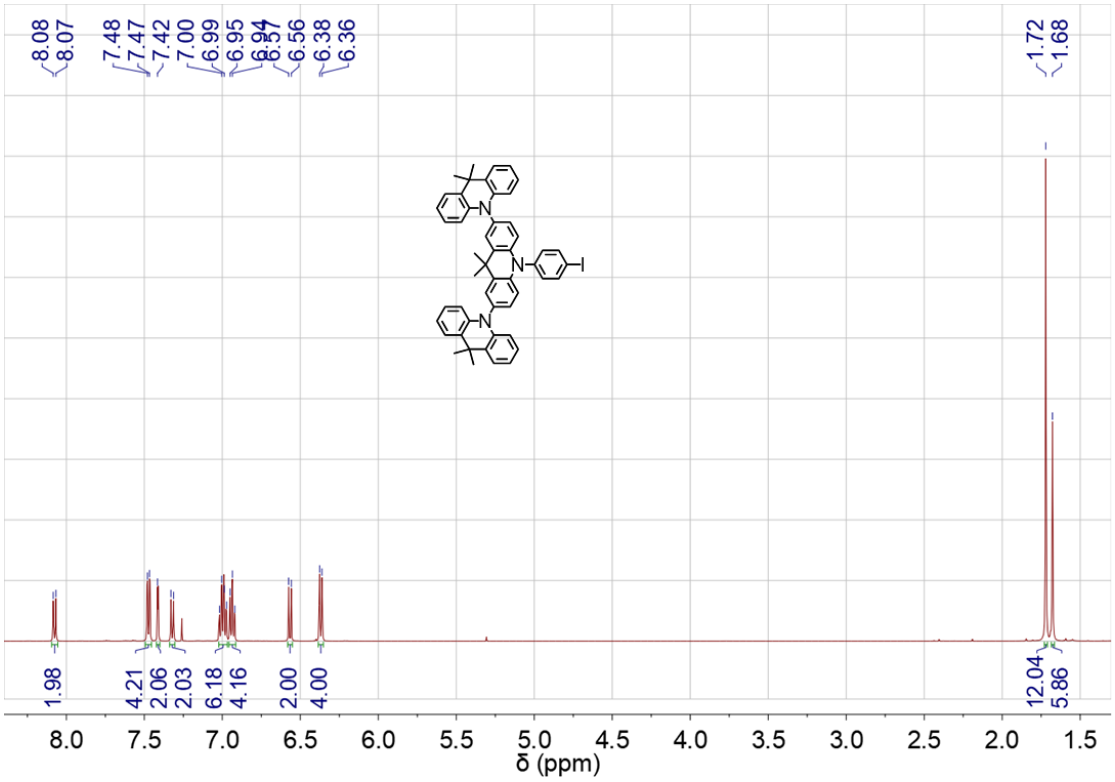

Figure S14. ^{1}H NMR spectrum of **2**.

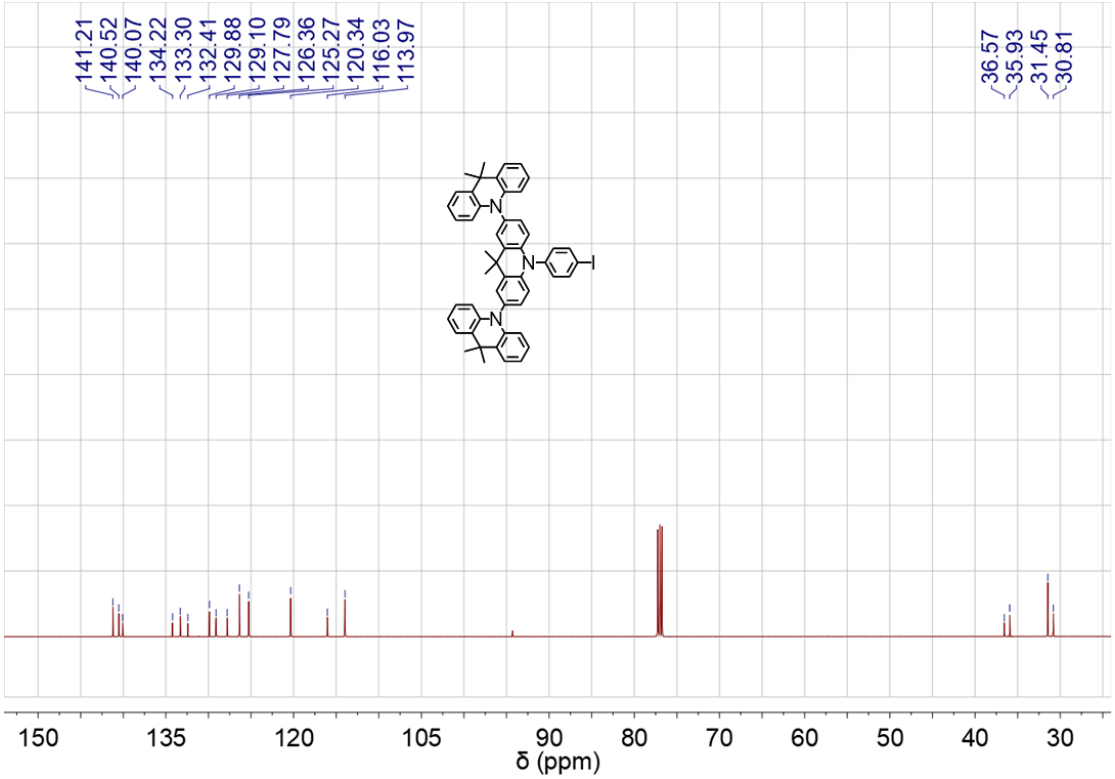

Figure S15. ^{13}C NMR spectrum of **2**.

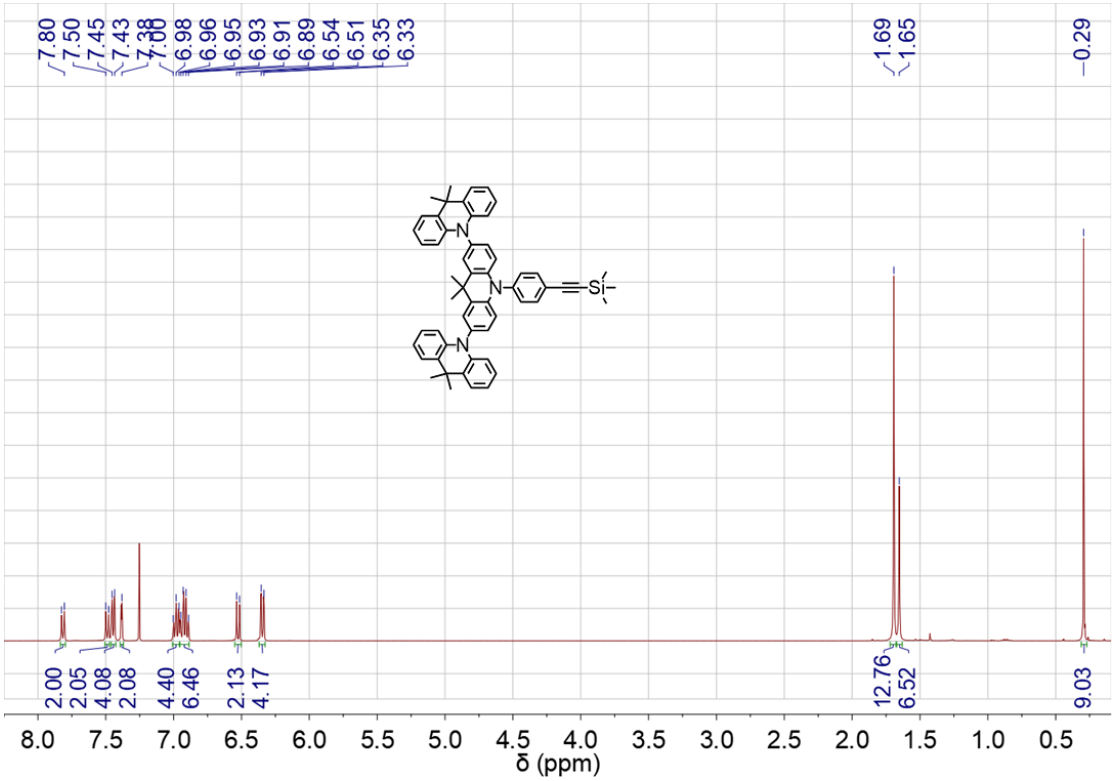

Figure S16. ^{1}H NMR spectrum of **3**.

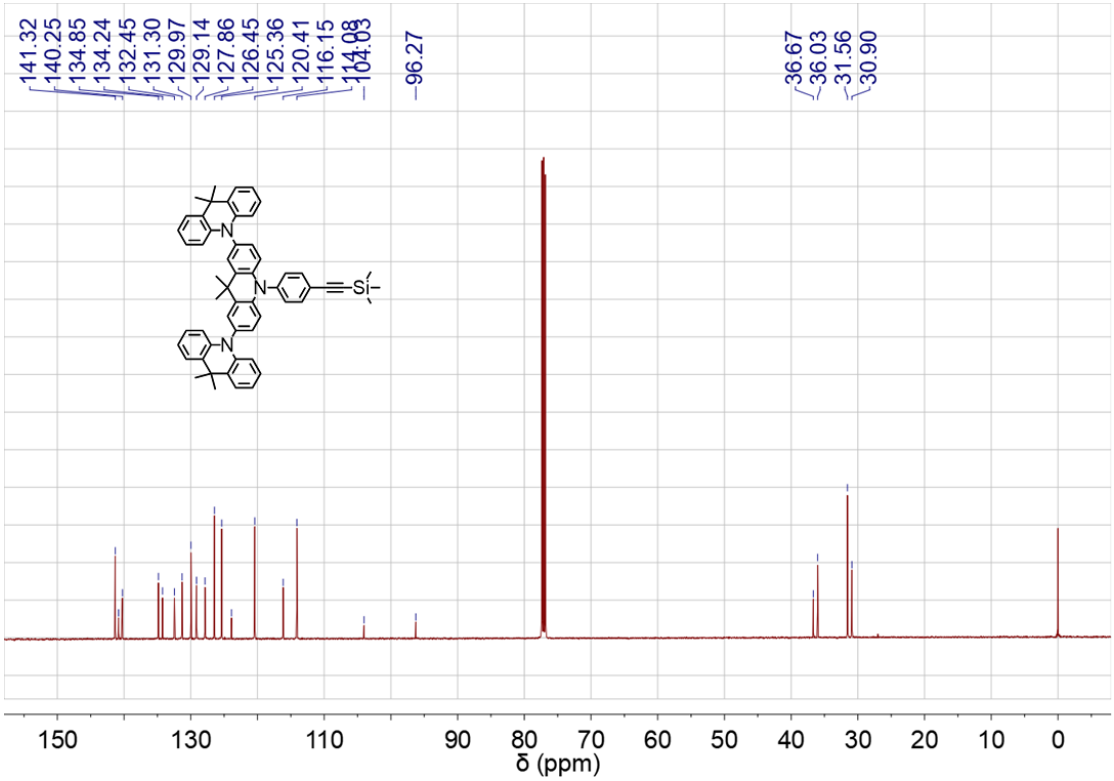

Figure S17. ^{13}C NMR spectrum of **3**.

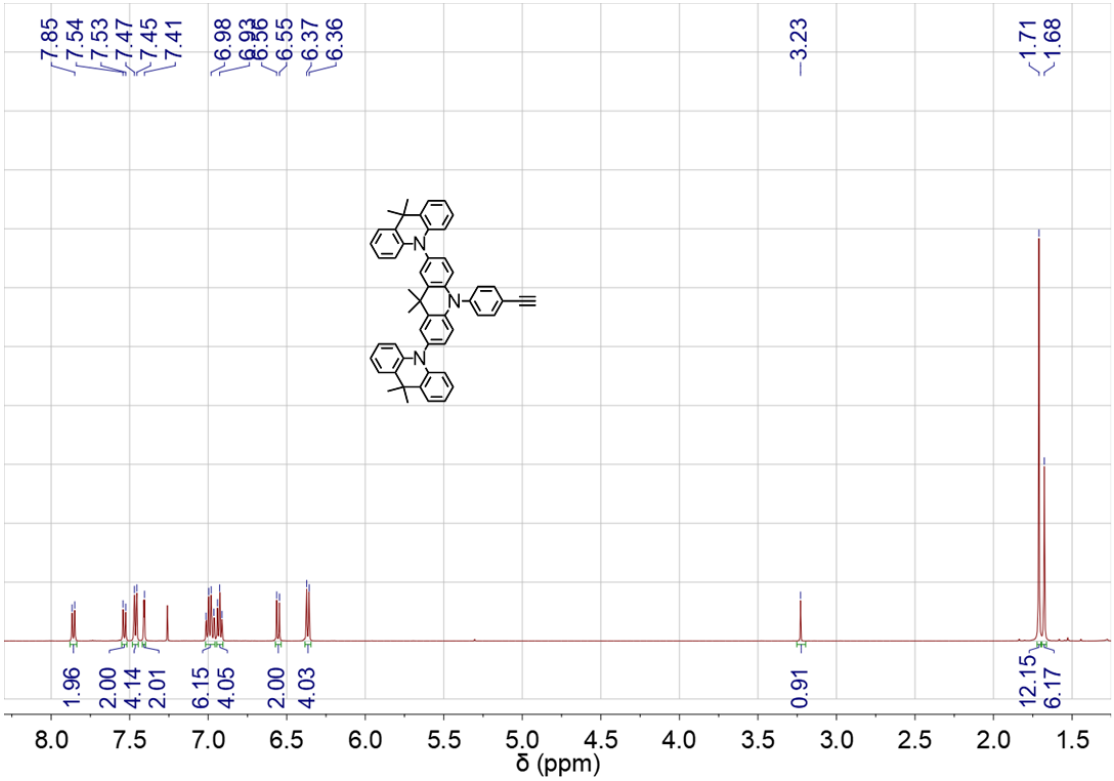

Figure S18. ^{1}H NMR spectrum of **4**.

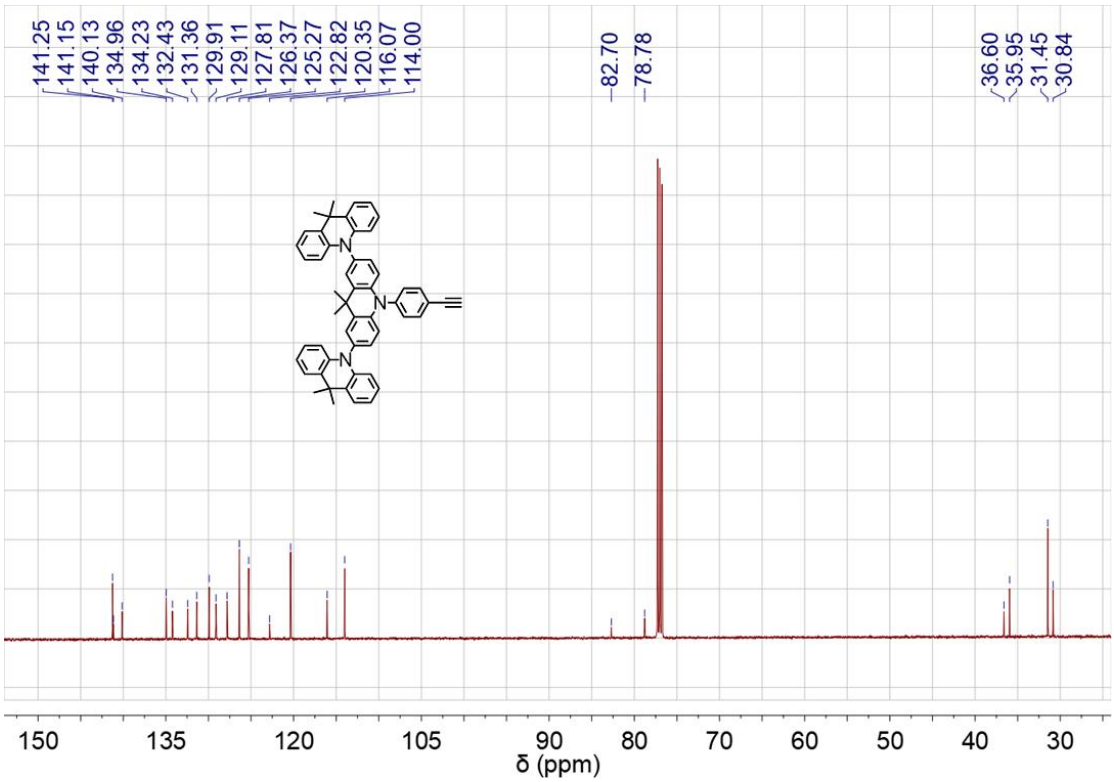

Figure S19. ^{13}C NMR spectrum of **4**.

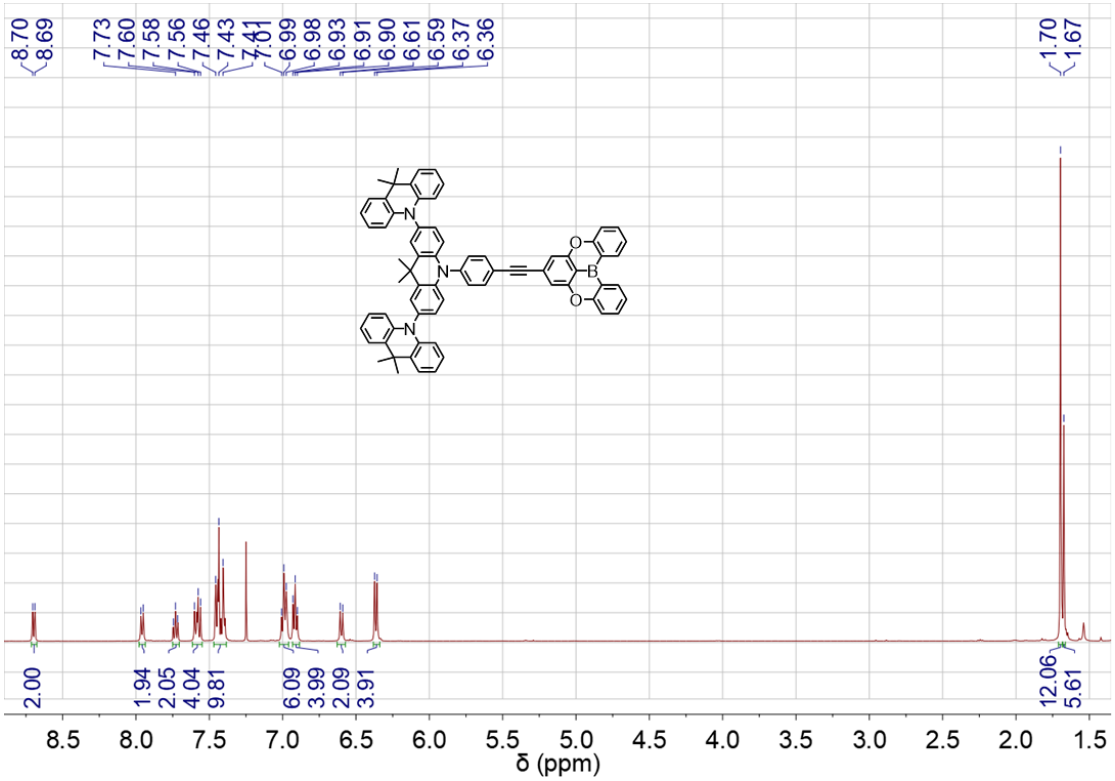

Figure S20. ^{1}H NMR spectrum of **6a**.

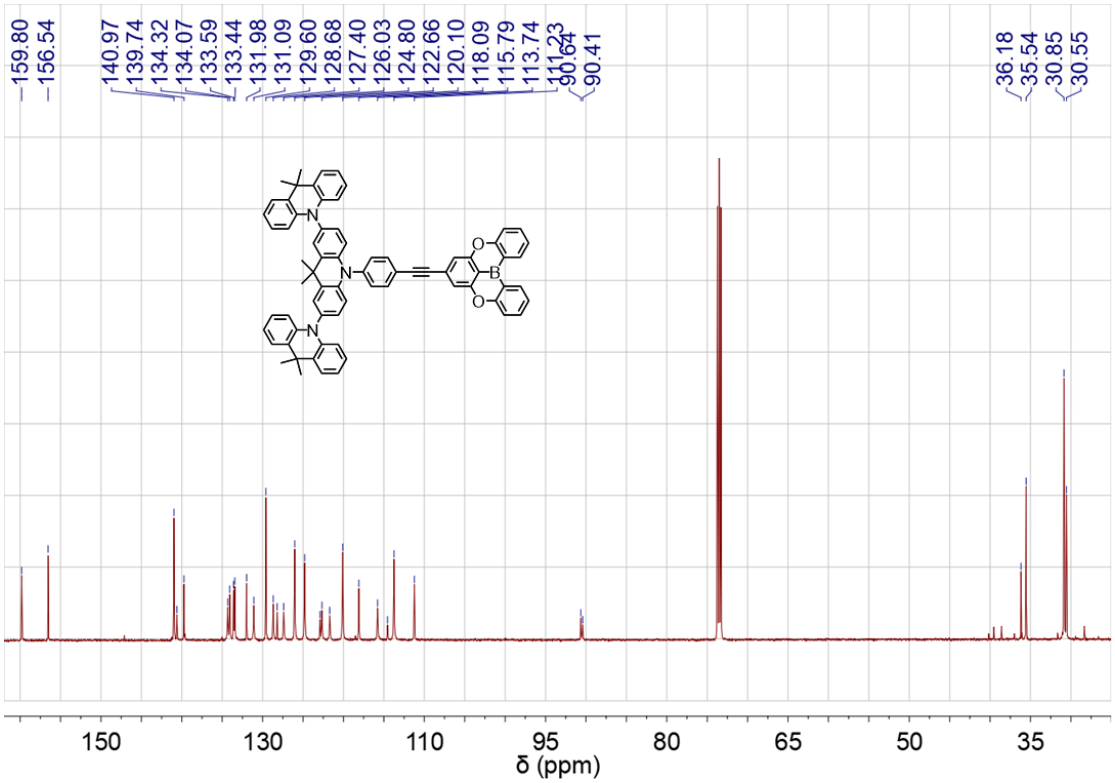

Figure S21. ^{13}C NMR spectrum of **6a**.

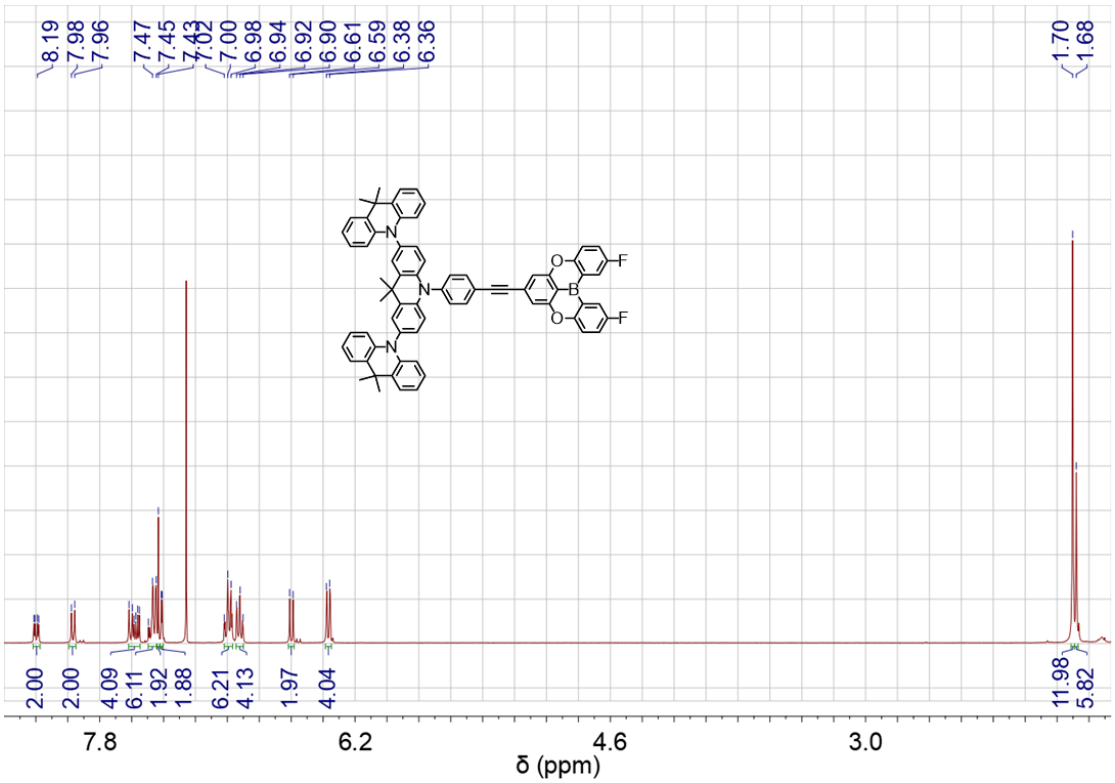

Figure S22. ^{1}H NMR spectrum of **6b**.

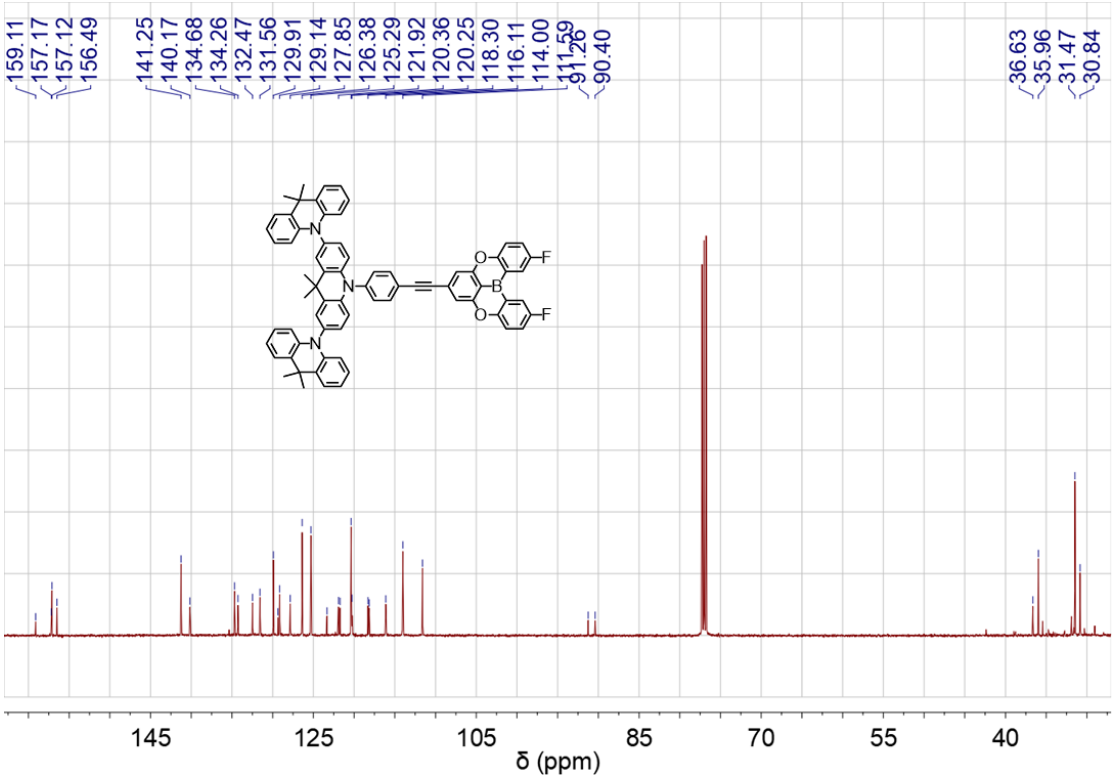

Figure S23. ^{13}C NMR spectrum of **6b**.

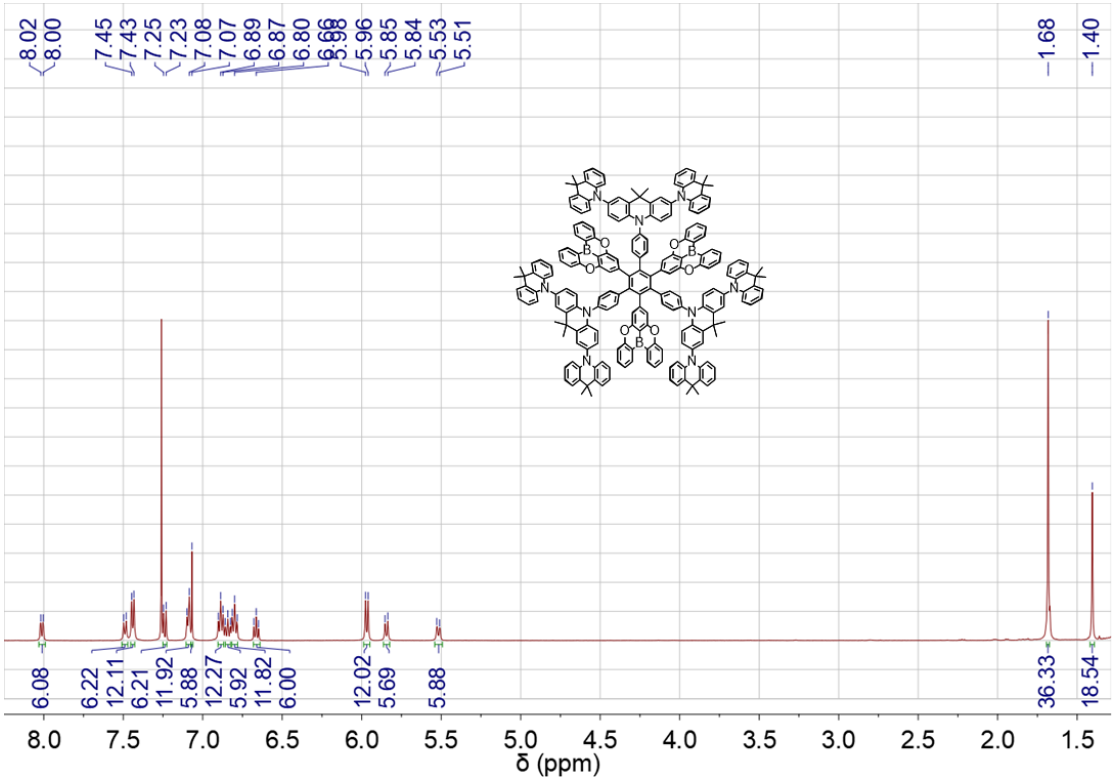

Figure S24. ^{1}H NMR spectrum of TAcBO-H.

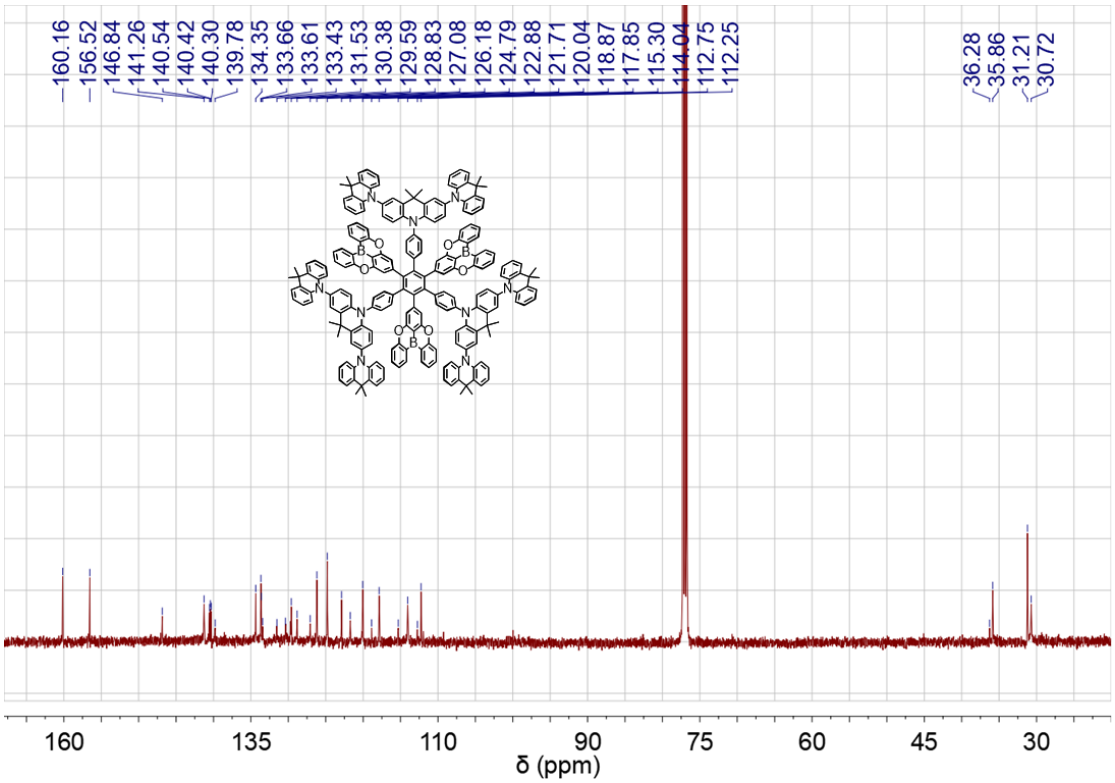

Figure S25. ^{13}C NMR spectrum of TAcBO-H.

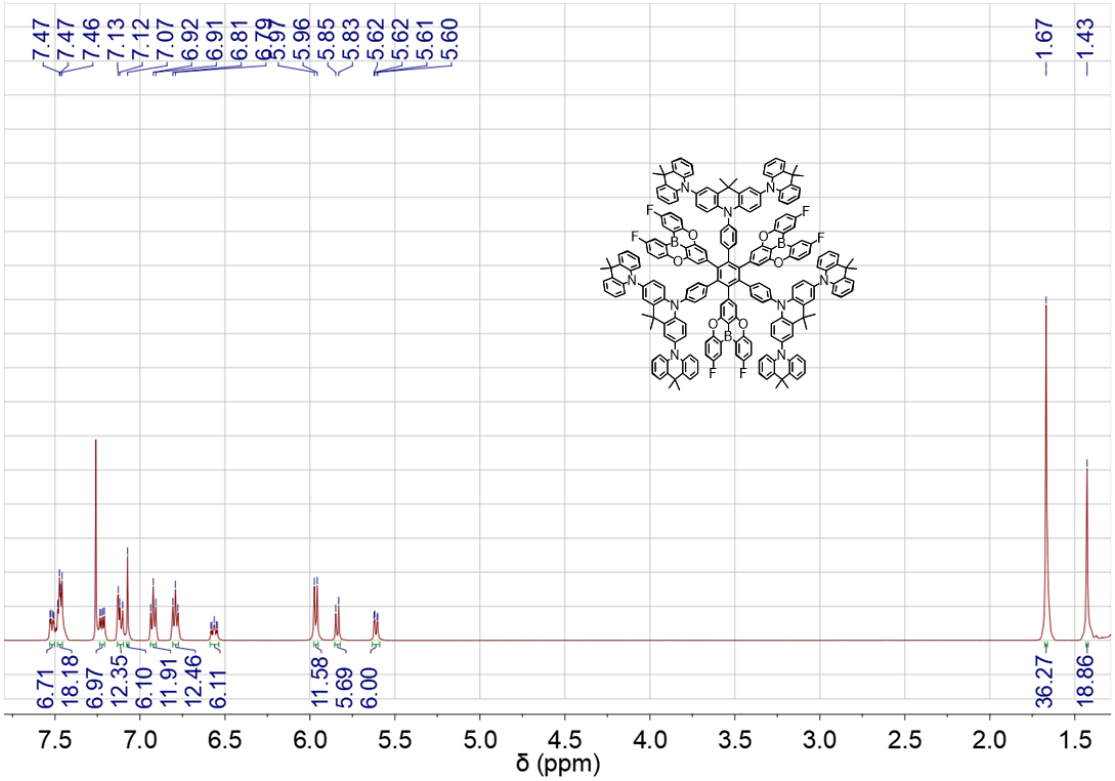

Figure S26. ^{1}H NMR spectrum of TAcBO-F.

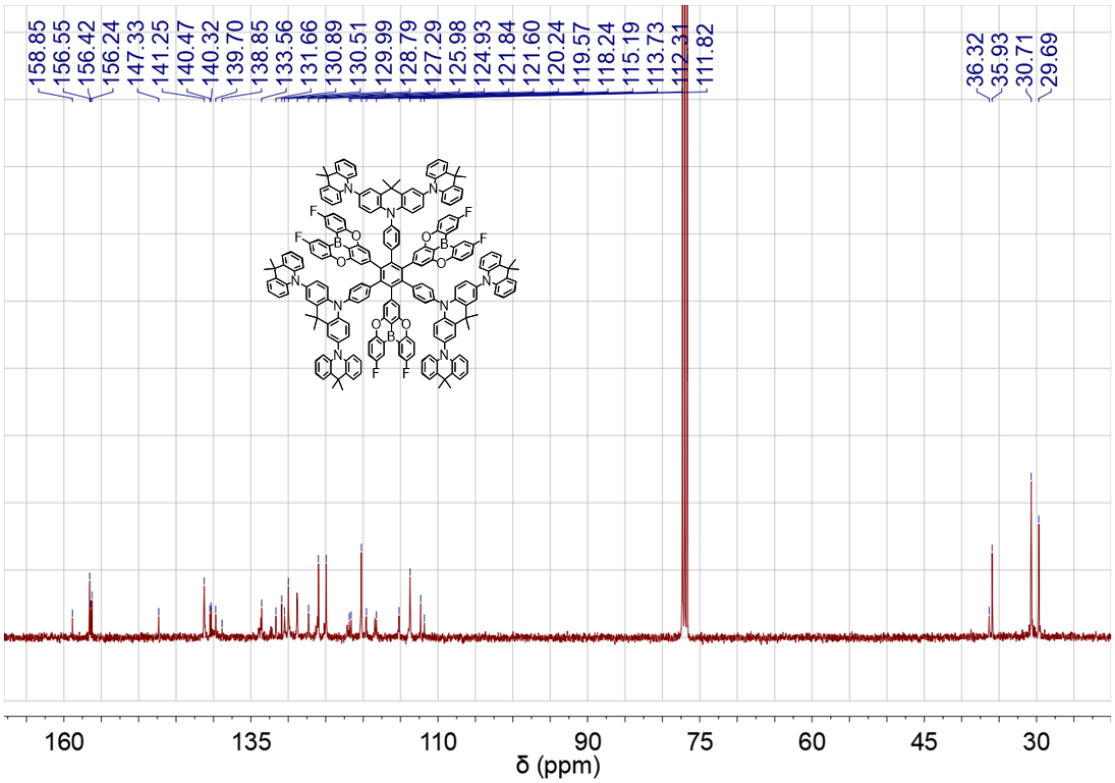

Figure S27. ^{13}C NMR spectrum of TAcBO-F.